Mon. Not. R. Astron. Soc. **385,** 430–444 (2008) doi:10.1111/j.1365-2966.2008.12851.x

Seismological studies of ZZ Ceti stars – I. The model grid and the application to individual stars

B. G. Castanheira[1,2⋆] and S. O. Kepler[1]

[1] *Departamento de Astronomia, Universidade Federal do Rio Grande do Sul, Av. Bento Gonçalves 9500 Porto Alegre 91501-970, RS, Brazil*
[2] *Institüt fur Astronomie, Türkenschanzstr. 17, A-1180 Wien, Austria*

Accepted 2007 December 12. Received 2007 December 11; in original form 2007 November 2

ABSTRACT

We calculate and explore an extensive adiabatic model grid for pulsating white dwarfs with hydrogen-dominated atmospheres, the ZZ Ceti stars. We also compared the computed modes with the observed ones for five ZZ Ceti stars that are a representative sample of the whole class of pulsators. We describe our new approach for seismological studies, using the relative observed amplitudes to give weights for the periods in the fit and the external mass and temperature determinations as a guide. Our seismological study is clear evidence that seismology is indeed a powerful tool in the study of stellar structure and evolution.

Key words: stars: individual: ZZ Ceti stars – stars: variables: other – white dwarfs.

1 INTRODUCTION

Because of the $\kappa-\gamma$ mechanism and/or convection driving, white dwarfs pulsate in three different instability strips, depending on the chemical element that drives pulsation. The 142 currently known DA variables (or ZZ Ceti stars) comprise the most numerous class of pulsating white dwarfs. These stars have hydrogen atmospheres and are confined in an observational narrow instability strip between 10 800 and 12 300 K. It is essential to note that pulsation is a phase every white dwarf goes through, that is, the properties we measure for pulsating stars apply to white dwarfs as a whole. The other two classes are the DB variables, with helium-rich atmospheres, and the DO variables, the hotter pulsators, with roughly a dozen of known pulsators in each class. Their temperatures range from 20 000 to 30 000 K and 75 000 to 170 000 K, respectively.

Pulsating white dwarfs constitute the largest population of variable stars, even though we can only detect the nearest ones because of their intrinsic faintness. Despite the relatively small number of known pulsators, their studies have extremely important astrophysical implications. Pulsations probe the internal structure of white dwarfs, as each pulsation mode yields an independent measurement of their interiors. Fundamental properties of the stars, such as mass, can be derived from just a few pulsation periods (Fontaine et al. 1991; Bradley & Winget 1994). If many modes are excited, the structure and composition of the white dwarfs can be determined in detail and with high precision (Winget et al. 1994; Kepler et al. 2003). Since they constitute the evolutionary end point of 95–98 per cent of all stars, information on their internal structure and composition provide a critical test for stellar evolution models, including the double shell burning phase at the asymptotic giant branch and mass-loss rates. As the periods of a pulsating white dwarf change slowly as the star cools, their rate of change measures the stellar cooling rate (e.g. Kepler et al. 2005), allowing the calibration of theoretical calculations. The cooling rates constrain in turn such properties as the rate of crystallization in the white dwarf core (Kanaan et al. 2005; Winget et al. 1997), plasmon–neutrino interaction cross-sections (Kawaler et al. 1986; Winget et al. 2004), and even axion masses (Córsico et al. 2001; Kim, Montgomery & Winget 2006). Coupled with the white dwarf luminosity function, the cooling rates yield a star formation history for the Galactic disc and, in principle, the age of the oldest disc and halo components (Winget et al. 1987; Hansen et al. 2002, 2007; Kalirai et al. 2007).

The ZZ Ceti stars can be separated in three groups: hot, intermediate and cool. The hot ZZ Ceti stars have only a few modes excited to visible amplitudes, all of them with short periods (smaller than 300 s), small amplitudes (from 1.5 to 20 mma), and the power spectrum does not change substantially from season to season. These stars define the blue edge of the ZZ Ceti instability strip. The cool ZZ Ceti stars are at the opposite side of the strip, showing a very rich pulsational spectra of high-amplitude modes (up to 30 per cent) and longer periods (up to 1500 s). The modes interfere with each other, causing dramatic changes in the pulsational spectra, but in general, the total amount of energy transported by pulsation is conserved. There are also a few red edge ZZ Ceti stars with long periods of low amplitude, representing the stage when the star is ceasing to pulsate. The intermediate ZZ Ceti stars have characteristics between the hot and the cool groups.

In this paper, we start by a detailed investigation on the seismological model grid, followed by the application of a new method of seismology to five ZZ Ceti stars. These stars are a representative sample of the whole class of the ZZ Ceti stars.

⋆E-mail: castanheira@astro.univie.ac.at

2 THE SEISMOLOGICAL MODELS

2.1 Calculating the models

The starting point to calculate the evolutionary model is a quasi-static pre-white dwarf model. The internal structure of white dwarfs with $T_{\rm eff} \sim 12\,000$ K has been sufficiently modified due to cooling, stellar contraction, and chemical diffusion, so that using a hot polytrope static model is equivalent to using models evolved from all the previous phases. The cooling sequence of those polytropes converge to the same structure obtained from self-consistent models even at temperatures above the observed pulsational instabilities for degenerate core atmosphere (e.g. Wood 1990).

We used the White Dwarf Evolutionary Code described in details by Lamb & van Horn (1975) and Wood (1990), to evolve the starting model until the desired temperature. This code was originally written by Martin Schwarzschild, but has been modified and updated by many astronomers (Montgomery 1998, and references therein). The equation of state for the core of our models is from Lamb (1974) and for the envelopes from Fontaine, Graboske & van Horn (1977). We used the updated opacity OPAL tables (Iglesias & Rogers 1996), neutrino rates of Itoh et al. (1996), and ML2/α = 0.6 mixing length theory of Bohm & Cassinelli (1971). The core evolution calculations are self-consistent, but the envelope was treated separately. The core and the envelope are stitched together, fulfilling the boundary conditions in the interface. The transitions between the layers are consistent with time-diffusion, following Althaus et al. (2003), especially for the transition zone between hydrogen (H) and helium (He).

2.2 Grid dimensions

We calculated an extensive adiabatic model grid for the pulsation modes, varying four quantities: $T_{\rm eff}, M, M_{\rm H}$ and $M_{\rm He}$. The whole grid was generated from a starting polytrope of $M = 0.6\,{\rm M}_{\odot}$, using homology transformations to obtain models with masses from 0.5 to 1.0 $\rm M_{\odot}$, in steps of 0.005 $\rm M_{\odot}$, initially. The effective temperature ($T_{\rm eff}$) varies from 10 600 to 12 600 K, in steps of 50 K. The upper H and He layer mass values are 10^{-4} and $10^{-2}\,M_{*}$, respectively; above these limits, nuclear reactions would excite g-mode pulsations in the planetary nebula nuclei variables by the ϵ mechanism, which are not observed (Hine 1988). The lower H and He layer mass values are $10^{-9.5}\,M_{*}$ (the minimum H amount to be detected in a DA white dwarf spectra) and $10^{-3.5}\,M_{*}$, respectively.

2.3 Core composition: C/O

Varying the core composition introduces three parameters in the fit: the abundance itself from the uncertain C(α, γ)O reaction rate (Metcalfe 2005) and the two extreme points of the function that better describes the transition zone. We chose a homogeneous core of 50:50 C/O, for simplicity. In Fig. 1, we show the variation in period with O abundance for the first three $\ell = 1$ overtones. We calculated a representative model of a star in the middle of the instability strip, $T_{\rm eff} = 11\,600$ K, with mass close to the DA white dwarf mean distribution, $M = 0.6\,{\rm M}_{\odot}$ (e.g. Kepler et al. 2007), and canonic values for H and He layer masses, $M_{\rm H} = 10^{-4}\,M_{*}$ and $M_{\rm He} = 10^{-2}\,M_{*}$. The change is only a few seconds when the O core

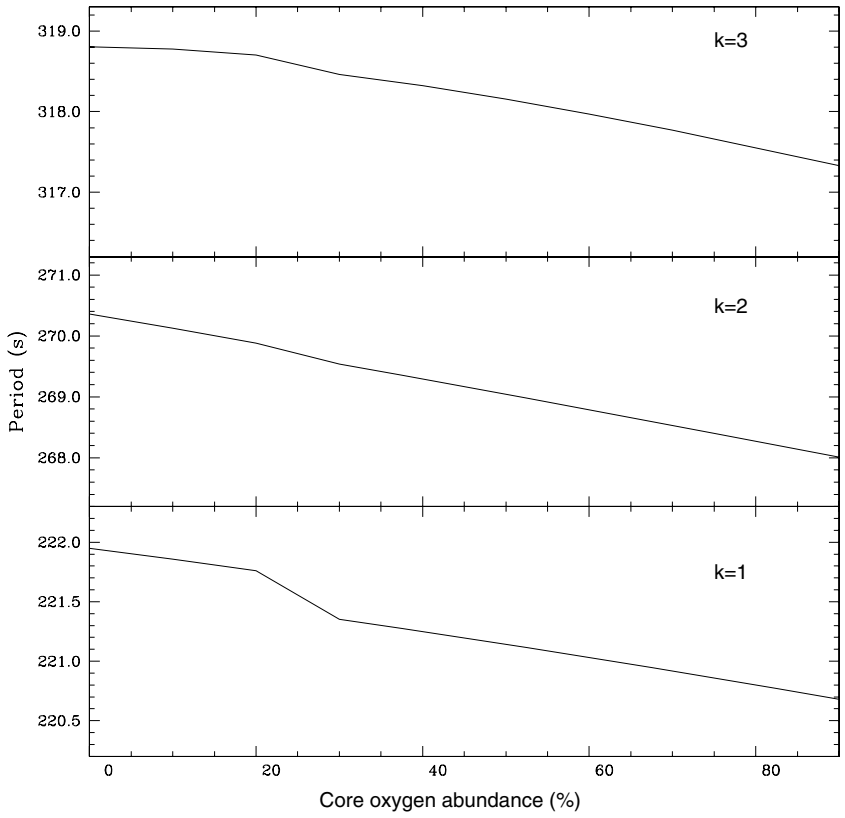

Figure 1. Variation in the first three $\ell = 1$ overtones changing the core abundances, for a model with $T_{\rm eff} = 11\,600$ K, $M = 0.6\,{\rm M}_{\odot}$, $M_{\rm H} = 10^{-4}\,M_{*}$ and $M_{\rm He} = 10^{-2}\,M_{*}$. In the lower panel is the variation for the $k = 1$ mode, in the middle panel for $k = 2$, and in the upper panel for $k = 3$.

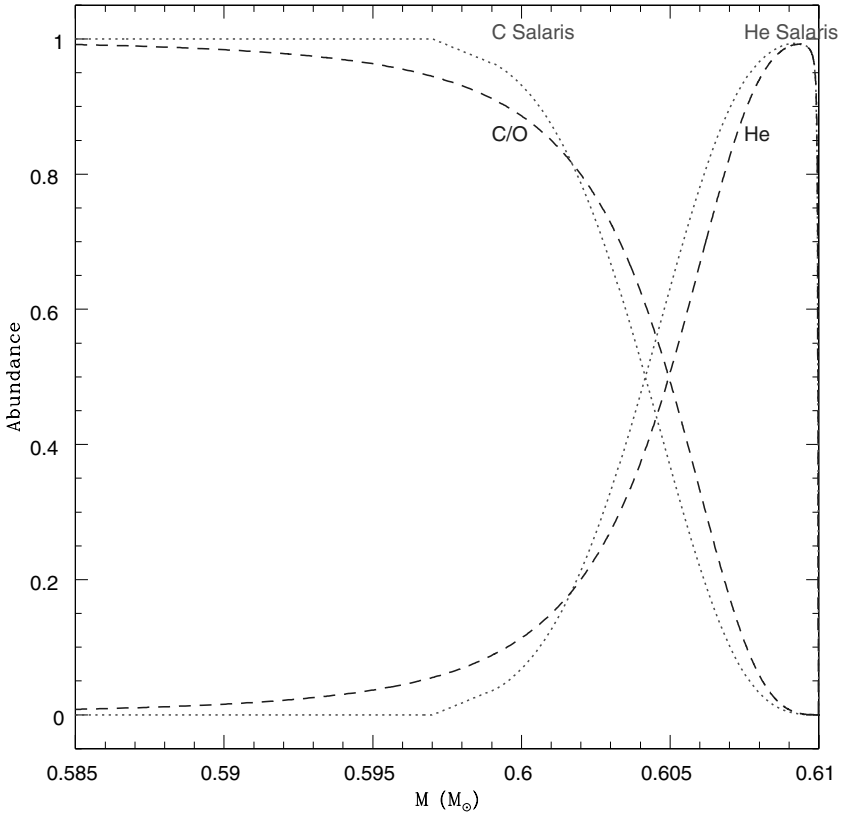

Figure 2. Comparison between Salaris profile (dotted red line) and our choice of homogeneous C/O = 50:50 core (dashed blue line). The positions of the transitions are different, causing differences in the calculated modes, which are trapped within these zones. However, the differences can be compensated by changing the thickness of the He layer.

abundance varies from 0 to 90 per cent (the complementary quantity is C)!

We also investigated the shape of the transition zones when a different profile is used. In Fig. 2, we show the abundance variation as a function of mass. The Salaris profile (Salaris et al. 1997) was derived from self-consistent models, and the simple profile is the one we used in our main grid. Both models were calculated for $T_{\rm eff} = 12\,000\,{\rm K}, M = 0.61\,{\rm M}_{\odot}, M_{\rm H} = 10^{-4}\,M_{*}$ and $M_{\rm He} = 10^{-2}\,M_{*}$. Clearly, the transition zones between the core and the He outer envelope are in different positions; therefore, the trapped modes in these cavities are necessarily different. Because the ZZ Ceti stars pulsate with only a few modes, we decided to use a fixed homogeneous C/O 50:50 core to decrease the number of model parameters, but still be consistent with the reaction rate uncertainty. The price paid for this choice is that the He layer mass determinations are uncertain. The differences in the shape of the transition zone can be compensated by changes in the thickness of the He layer. The Salaris profile introduces a more complicated than a linear decrease in the O profile in the outer layers (see fig. 2. of Metcalfe 2005). This effect potentially changes the calculated trapped modes in the models. However, because the ZZ Ceti stars pulsate in only a few modes, we did not include the changes in the core profile in our fit.

For high- and low-mass white dwarfs, core composition plays an important role and should be slightly different, but these stars are a small fraction ($\leqslant$30 per cent) of all known ZZ Ceti stars, and white dwarfs in general. In the few cases, that mass determinations are precise enough, it is necessary to compute models for other C/O proportions (see Section 3.5).

2.4 Exploring the model grid

The ZZ Ceti stars at the blue edge of the instability strip pulsate with only a few short-period modes, the first overtones. We show the changes in the period of the first overtone as a function of the H layer mass thickness in Fig. 3, for a model with $T_{\rm eff} = 12\,000\,{\rm K}$, $M = 0.6\,{\rm M}_{\odot}$ and $M_{\rm He} = 10^{-2}\,M_{*}$.

The first observation is the presence of avoided crossings in the models, which occurs when a mode assumes the properties of the immediate next k mode. The consequence is a variable period spacing (ΔP), depending on the thickness of the H layer.

Consider a hypothetical star that pulsates with an $\ell = 1$ mode at 217.5 s. For the model with $T_{\rm eff} = 12\,000\,{\rm K}, M = 0.6\,{\rm M}_{\odot}$ and $M_{\rm He} = 10^{-2}\,M_{*}$, there are two possible solutions: $M_{\rm H} = 10^{-7.5}\,M_{*}$ if $k = 1$ or $M_{\rm H} = 10^{-4}\,M_{*}$ if $k = 2$ (see Fig. 3). On the other hand, if the atmosphere parameters have a different value, for instance, $T_{\rm eff} = 11\,000\,{\rm K}$ and $M = 0.7\,{\rm M}_{\odot}$ (solid line in Fig. 3), the best solution would be $M_{\rm H} = 10^{-6.5}\,M_{*}$, if the mode is $\ell = 1, k = 2$. Nevertheless, an $T_{\rm eff} = 11\,000\,{\rm K}$ solution can be excluded, because this is a typical temperature of a red edge pulsator, while the observed period is typical of a blue edge pulsator. This simple example illustrates the degeneracy of our model grid. It is thus necessary to detect as many modes as possible to find a unique solution for the stellar structure of our targets.

In Fig. 4, we show the changes in the first $\ell = 1$ and 2 overtones with stellar mass, for a model with $T_{\rm eff} = 12\,000\,{\rm K}, M_{\rm H} = 10^{-4}\,M_{*}$ and $M_{\rm He} = 10^{-2}\,M_{*}$. For the previous $\ell = 1$ 217.5 s pulsator,

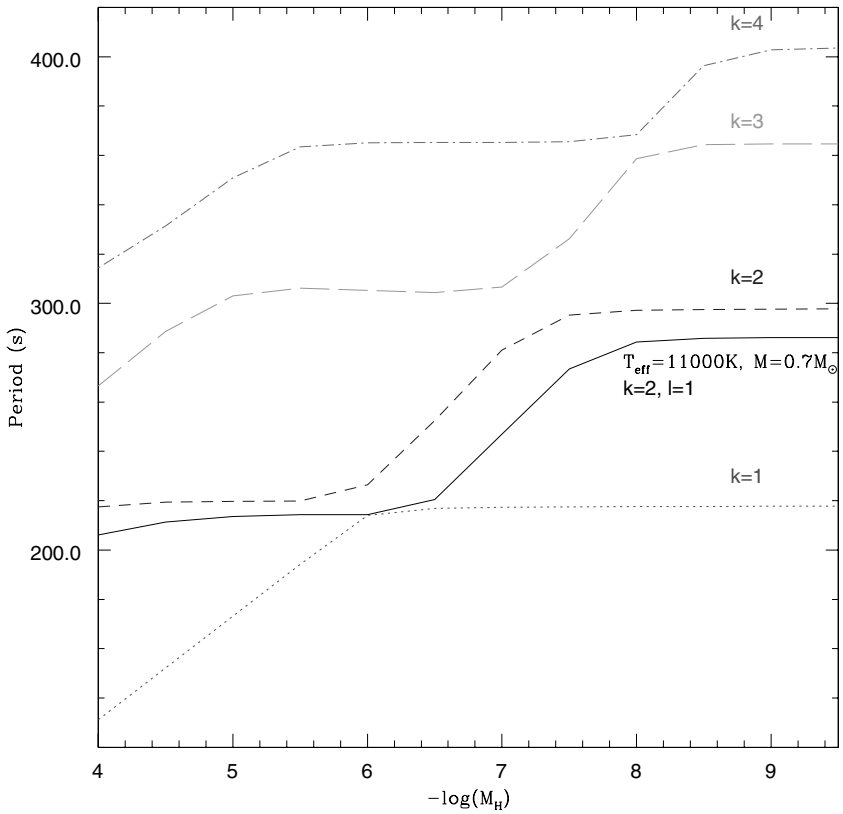

Figure 3. Variation in the first $\ell = 1$ overtones with the mass of the H envelope for a model with $T_{\rm eff} = 12\,000$ K, $M = 0.6\,{\rm M}_{\odot}$ and $M_{\rm He} = 10^{-2}\,M_{*}$. The dotted (red) line is for the mode $k = 1$, the dashed (blue) line for $k = 2$, the long-dashed (green) line for $k = 3$, and the dot–dashed (magenta) line for $k = 4$. The continuous (black) line is the $k = 2\,\ell = 1$ mode variation, but for a model with $T_{\rm eff} = 11\,000$ K, $M = 0.7\,{\rm M}_{\odot}$ and $M_{\rm He} = 10^{-2}\,M_{*}$. Both models are for a homogeneous C/O =50:50 core.

the possible solutions are $0.60\,{\rm M}_{\odot}$ if $k = 2$, $0.74\,{\rm M}_{\odot}$ if $k = 3$, and $0.86\,{\rm M}_{\odot}$ if $k = 4$.

We also computed models for $\ell = 2$, 3, and 4 modes, despite the fact they are less likely to be observed in the optical, because of the geometrical cancellation (Robinson, Kepler & Nather 1982). Robinson et al. (1995), Kepler et al. (2000) and Castanheira et al. (2004) studied the chromatic amplitude variation and conclude that most of the observed ZZ Ceti star modes are $\ell = 1$. The results of Kotak, van Kerkwijk & Clemens (2004) and Clemens, van Kerkwijk & Wu (2000) point to the same conclusion, even though their Keck optical data sampled only a small wavelength range. That is an important point, because there are more excitable $\ell = 2$ modes than $\ell = 1$ in any model (see Fig. 4). If our hypothetical star pulsates with an $\ell = 2$ mode instead, the best fits would be $0.61\,{\rm M}_{\odot}$ if $k = 4$ and $0.71\,{\rm M}_{\odot}$ if $k = 5$.

Fig. 5 shows the variation in the first $\ell = 1$ overtones as a function of $T_{\rm eff}$, for models with $M = 0.6\,{\rm M}_{\odot}$, $M_{\rm H} = 10^{-4}\,M_{*}$ and $M_{\rm He} = 10^{-2}\,M_{*}$. The most important result is that the modes are getting longer as the models cool down. Physically, we are measuring the core cooling, which is the dominant effect in the ZZ Ceti phase.

At the blue edge, the lower values of k are excited (Winget, van Horn & Hansen 1981; Brassard et al. 1991). In Fig. 6, we show the period spacing ΔP between the two first overtones ($k = 1$ and 2) for $\ell = 1$ and 2. For stars with $M \sim 0.6\,{\rm M}_{\odot}$, if close modes could not be explained by avoided crossings, a period spacing smaller than around 50 s should indicate $\ell = 2$.

3 SEISMOLOGY OF INDIVIDUAL STARS

3.1 G117−B15A: our test star

Since the discovery of its variability (McGraw & Robinson 1976), G117−B15A was considered the most-regular ZZ Ceti. Its light curve is nearly sinusoidal, showing mean light variations with $\simeq$2 per cent amplitude. Due to the mode stability, Kepler et al. (2005) measured the rate of change in the main mode at 215 s, with a precision better than 10^{-15} s s^{-1}. G117−B15A is the most-precise optical clock known.

G117−B15A pulsates with only three independent low-amplitude modes, showing also the harmonic of the main mode and linear combinations between the modes (Kepler et al. 1982). In Table 1, as an example, we list the average values for all periodicities detected in observations with the Argos camera (Nather & Mukadam 2004) at the 2.1-m telescope at the McDonald Observatory.

We used G117−B15A as a test of our seismological analysis for two main reasons. First, this star shows a very simple pulsation spectrum, but more than one mode is excited. Secondly, there are published seismological studies, which can be used to test the validity of our approach.

Our seismological study starts with a literature search for all available information about the star. Besides more than 30 yr of time-series photometry (Kepler et al. 2005), there are independent measurements of the atmospheric properties ($T_{\rm eff}$ and $\log g$) of G117−B15A, from different techniques, summarized in Table 2.

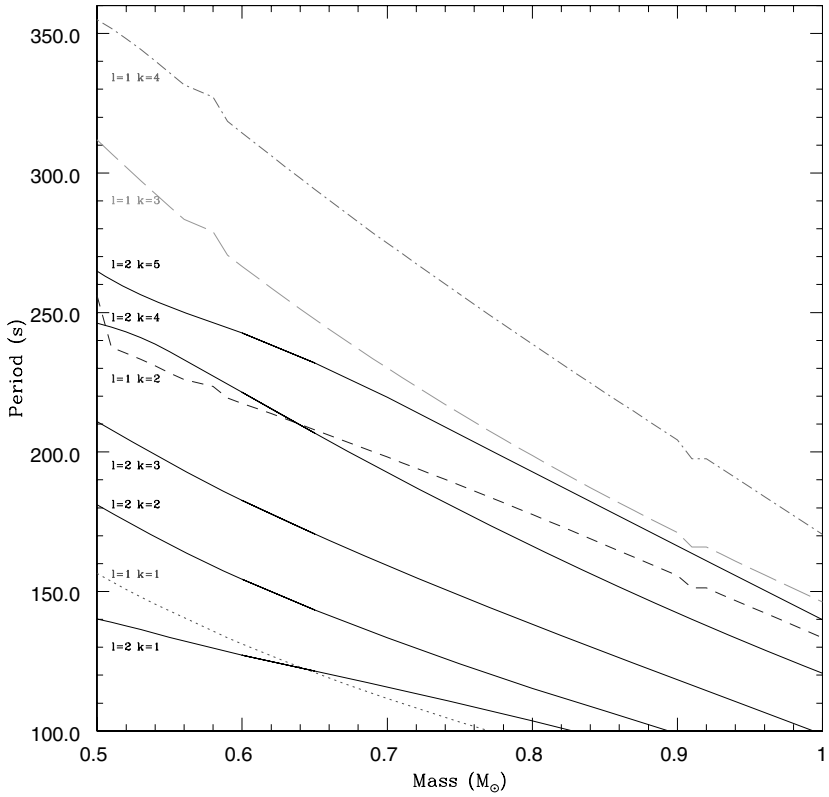

Figure 4. Variation in the first overtones for a model with $T_{\rm eff} = 12\,000$ K, $M_{\rm H} = 10^{-4}\,M_*$ and $M_{\rm He} = 10^{-2}\,M_*$ as a function of mass. The solid lines are for models with $\ell = 2$ and the other lines are for $\ell = 1$ modes. The first values of k are for shorter periods and the higher, for longer periods. For the same ℓ and k mode, the modes are shorter for higher mass values.

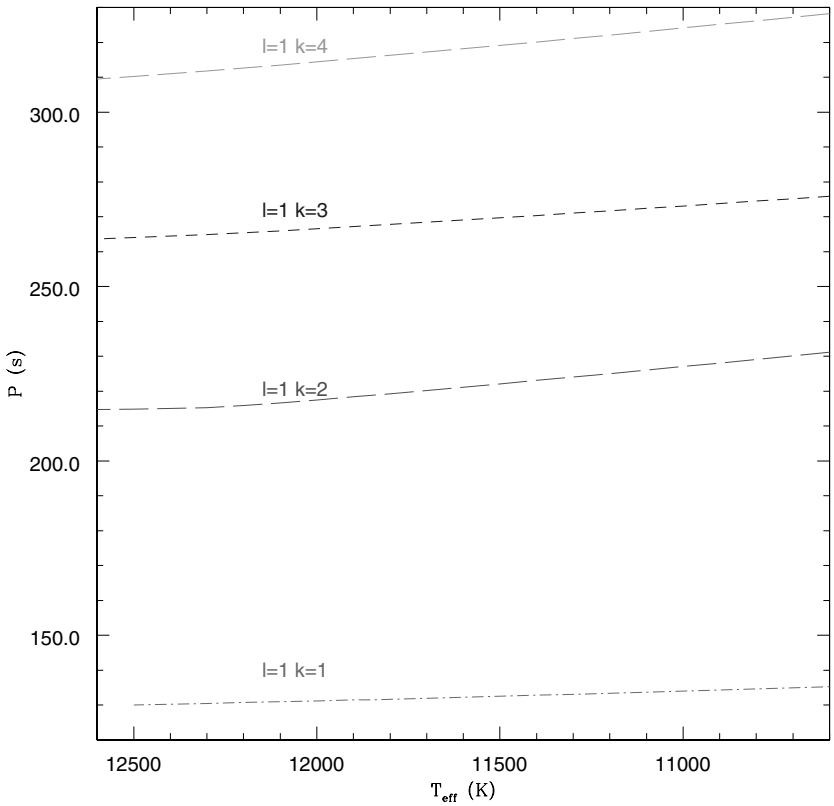

Figure 5. Variation in the first overtones for a model with $M = 0.6\,{\rm M}_{\odot}$, $M_{\rm H} = 10^{-4}\,M_*$ and $M_{\rm He} = 10^{-2}\,M_*$, as a function of $T_{\rm eff}$.

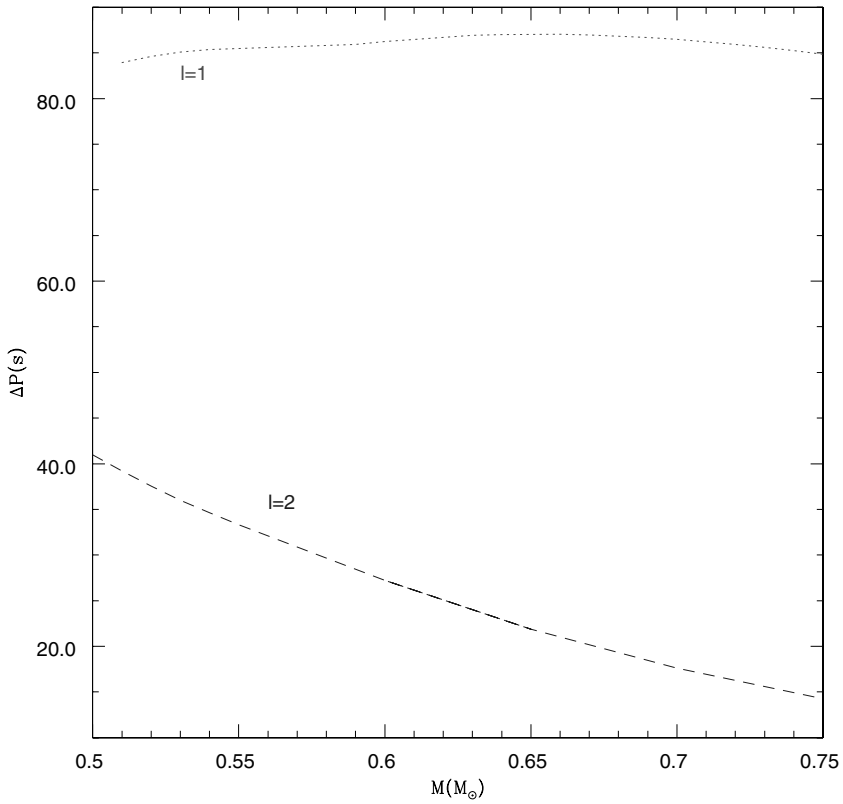

Figure 6. Period spacing between the two first overtones ($k = 1$ and 2) for $\ell = 1$ and 2 modes. The difference between higher ℓ modes is smaller in comparison to smaller ℓ modes, for a particular model.

Table 1. All detected periodicities for G117−B15A, with mode labelled as well as the linear combinations and the harmonic of the main mode, which are not fundamental modes of the star.

Period (s)	Amplitude (mma)	Identification
215.20	17.36	f1
270.46	6.14	f2
304.05	7.48	f3
107.7	1.65	2×f1
126.2	1.40	f1+f3
119.8	1.30	f1+f2

The differences among the published values can be explained by the intrinsic degeneracy between $T_{\rm eff}$ and $\log g$, which allows more than one combination of solutions.

As our models do not account for the excitation of linear combinations nor harmonics, it is very important to be sure that only normal modes are being used in the fit. For G117−B15A, the modes are identified in Table 1 as f_1, f_2 and f_3. To perform seismology, we compared the observed modes ($P_{\rm obs}$) with the computed ones ($P_{\rm model}$) by adding the square of the differences, similar to a χ^2 fit, according to the expression

$$S = \sum_{i=1}^{n} \sqrt{\frac{[P_{\rm obs}(i) - P_{\rm model}]^2 \times w_P(i)}{\sum_{i=1}^{n} w_P(i)}}, \quad (1)$$

where n is the number of observed modes and w_P is the weight given to each mode.

In order to give higher weight to the highest-amplitude mode, we choose to weigh the periods by the energy they transport, which is proportional to the observed amplitude square (A^2). Even though our model grid uses the adiabatic approximation and does not provide theoretical amplitudes, we are using the observed relative amplitudes to weigh our fits, to guarantee that the fit will be always dominated by high-amplitude modes. For G117−B15A, the periods and their respective normalized weights are 215.20, 270.46 and 304.05 s, and 0.13, 1.00 and 0.67.

At first, we have tried $\ell = 1$ for all modes. This choice is supported by previous observations of Robinson et al. (1995) and Kotak et al. (2004). We would have tried higher ℓ values if no solution was found, despite the fact that all chromatic amplitude changes to date

Table 2. Independent atmospheric determinations for G117−B15A.

Method	$T_{\rm eff}$ (K)	$\log g$ (cgs units)	M ($M_\odot$)	Spectroscopic reference
Optical spectra line profile technique (LPT)	11 630 ± 200	7.97 ± 0.05	0.59 ± 0.03	Bergeron et al. (2004)
UV spectra + V mag	11 900 ± 140	7.86 ± 0.14	0.53 ± 0.07	Koester & Allard (2000)
Gravitational reddening		8.00 ± 0.14	0.58 ± 0.08	Wegner & Reid (1991)

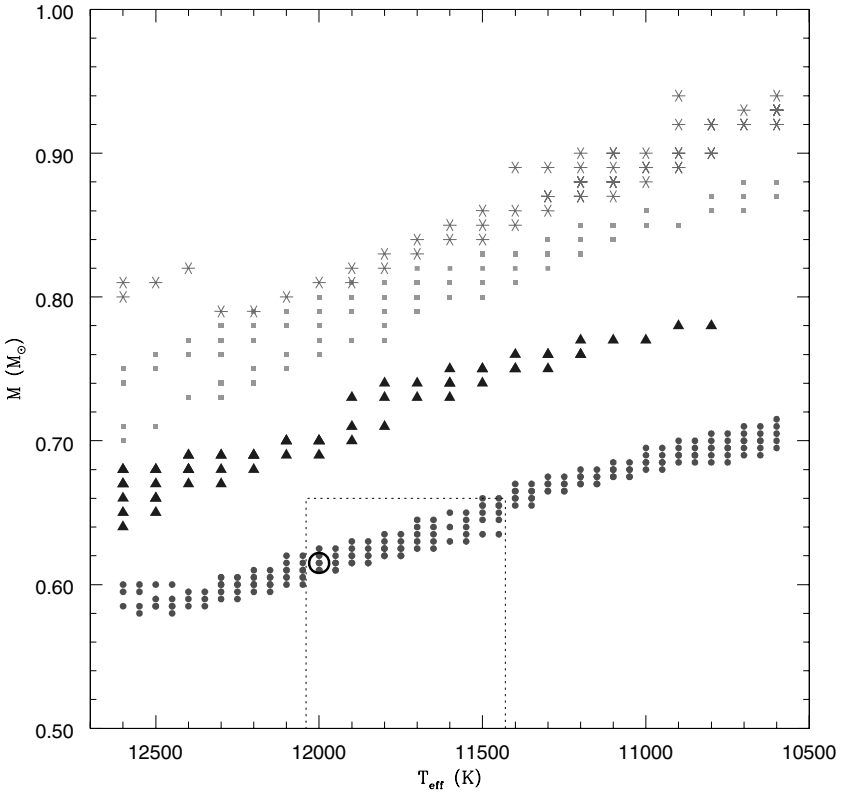

Figure 7. Results from comparison between the pulsation modes of the star G117−B15A and the models. The (red) circles are the solutions for $M_{\rm He} = 10^{-2}$ M_*, the (blue) triangles for $M_{\rm He} = 10^{-2.5}$ M_*, the (green) squares for $M_{\rm He} = 10^{-3}$ M_*, and the (magenta) asterisks for $M_{\rm He} = 10^{-3.5}$ M_*. The dotted line box limits the region of the independent temperature and mass determinations ($\pm$ 1σ) listed in Table 2 and the open circle shows the location of the minimum for this family of solutions.

Table 3. Seismological solutions for G117−B15A: absolute minima for each possible family of solutions in Fig. 7. Values in bold represent seismological solution that better agrees with external methods. All points are below S cut off.

Symbol in Fig. 7	$T_{\rm eff}$ (K)	M ($M_\odot$)	$-\log M_{\rm H}$	$-\log M_{\rm He}$	S (s)	Modes (ℓ, k)
(Red) Circles	**12 000**	**0.615**	**7**	**2**	0.67	215.3(1, 1), 275.0(1, 2) 302.1(1, 3)
(Blue) Triangles	11 500	0.75	5	2.5	0.97	215.1(1, 2), 265.1(1, 3) 308.0(1, 4)
(Green) Squares	12 600	0.71	7.5	3	0.73	215.4(1, 1), 266.0(1, 2) 301.6(1, 3)
(Pink) Asterisks	11 500	0.85	8.5	3.5	0.19	215.2(1, 1), 271.5(1, 2) 303.3(1, 4)

indicate that the modes are more likely $\ell = 1$ than higher ℓ for all ZZ Ceti stars (e.g. Kepler et al. 2000).

By comparing the observations and the models, we found several families of solution below the cut $S < 1.8$ s (the quadratic sum of the relative uncertainties). Fig. 7 shows the possible combinations of $T_{\rm eff}, M, M_{\rm H}$ and $M_{\rm He}$ below the S cut-off, and the minimum of each family is listed in Table 3.

Zhang, Robinson & Nather (1986) derived the following expression to calculate the uncertainties in the fit parameters:

$$\sigma^2 = \frac{d^2}{S - S_0}, \tag{2}$$

where d is the imposed step, S_0 is the absolute minimum, and S is the local minimum in a d difference between the quantities.

The mean uncertainties for the quantities we fit are $\sigma_{T_{\rm eff}} \sim 50$ K, $\sigma_M \sim 0.005\,{\rm M}_\odot$, $\sigma_{M_{\rm H}} \sim 10^{-0.5} M_*$ and $\sigma_{M_{\rm He}}$ $10^{-0.5}{\rm M}_*$, of the order of the spacings in the model grid. These values are the typical uncertainties in our seismological studies.

The final step is to identify which of the possible solutions correlates with the atmospheric determinations. From Table 2, the mass should be within the range 0.46–0.66 $\rm M_\odot$, which excludes all seismological high-mass solutions; only the first solution in Table 3 is consistent with the previous atmospheric determinations. In the same way, the spectroscopic temperature is within the range 11 430–12 040 K, which also agrees with this solution. Our seismological solution indicates that $T_{\rm eff}$ is hotter than determined by Bergeron et al. (2004), but consistent with the value from the ultraviolet (UV) spectra (see Table 2).

Alternatively to our procedure, Bradley (1998) applies his six-step recipe. The first step is to select seismological models consistent with spectroscopic mass and temperature. He uses a standard model with $M_{\rm He} = 10^{-2}\,M_*$ and C/O nominal profile. Afterwards, he adjusts $M_{\rm H}$ to obtain a mode with $\ell = 1, k = 1$ or 2 close to 215 s. He then refines $T_{\rm eff}$ and $M_{\rm H}$ to bring the 270-s mode into agreement. The next step is to use the 304-s mode to adjust C/O profile. Finally, he refines the adjustment even more and/or applies small changes to $M_{\rm H}, M_{\rm He}$, and in the core structure. He found that the mass of the H layer is either $M_{\rm H} = 10^{-4}\,M_*$ or $10^{-7}\,M_*$, depending on if the 215-s $\ell = 1$ mode is $k = 2$ or 1, respectively. His best result in mass is $0.60\,{\rm M}_\odot$, which agrees with spectroscopic values.

The code he used to calculate his models is basically the same as we used. However, his version used the trace element approximation, while our updated version uses a parametrization that mimics the results of time-dependent diffusion calculations (Althaus et al. 2003) to describe the transition zones. The biggest advantage of our seismological recipe is that we can explore all possibilities, avoiding local minima and error propagation if the spectroscopic determinations are uncertain.

Benvenuto et al. (2002) used realistic He, C and O profiles, calculated from previous stellar evolutionary phases, obtaining $T_{\rm eff} = 11\,800$ K, $M = 0.525\,{\rm M}_\odot$ and $M_{\rm H} = 10^{-3.83}\,M_*$, for G117−B15A. Their $T_{\rm eff}$ and mass are consistent with Koester & Allard (2000) determinations by fitting the UV spectrum.

Our seismological study of G117−B15A is in agreement with other approaches, encouraging us to apply the same technique to other ZZ Ceti stars.

3.2 G185−32: a rebel star

The exotic behaviour of G185−32 has been noted since the discovery of its variability (McGraw et al. 1981). The subharmonic ($3f_0/2$) and the second harmonic ($3f_0$) are excited and have comparable amplitudes to the main periodicity at $P = 215$ s (f_0) in the optical. Castanheira et al. (2004) identified the ℓ degree of at least five pulsation modes using chromatic amplitude differences. The subharmonic at 141.9 s was proposed to be a non-linear effect and the shortest periodicity at 70.9 s ($3f_0$) should be $\ell = 2$, probably $k = 1$.

Thompson et al. (2004) studied the UV (Kepler et al. 2000) and optical chromatic amplitude variations in the 142 s periodicity and proposed it as an $\ell = 4$ mode. In their model, even though $\ell = 4$ mode cancels itself over the visible hemisphere for almost all inclination values, the harmonic does not, because it has a different surface distribution, similar to lower ℓ modes. In this scenario, the harmonic would be allowed to have a higher amplitude than the fundamental mode.

Yeates et al. (2005) studied the amplitude ratios between harmonics and their parent modes, for hot ZZ Ceti stars, to constrain the ℓ index, based on Wu's (2001) theoretical predictions. They proposed the 141.9-s mode as an $\ell = 3$.

Pech & Vauclair (2006) suggest that G185−32 pulsates mainly with $\ell = 2$ modes. The 72.5-s mode was labelled by them as $\ell = 2, k = 1$ and used as a reference mode, even though it has never been observed as the dominant mode. They proposed that the 70.9, 148.5, 181.9, 212.8 and 215.7 s (the dominant periodicity in all data sets) modes are not real modes. The 141.9 s periodicity would be a superposition of a real $\ell = 2$ mode and the linear combination of two parent modes, with $\ell = 3$ and 4 or 5. The resulting amplitude of an $\ell = 2$ would be modified by the interference of the linear combinations. In this scenario, it would not be surprising that the 142-s chromatic amplitude variation does not follow the theoretical predictions. Their analysis does not take into account the relative amplitudes and assumes that the temperature and mass derived from optical spectra are accurate.

Bradley (2006) suggests yet another possibility: the modes at $P = 72.5$ and 141.9 s would be $\ell = 4, k = 2$ and $k = 8$, respectively. However, the high geometric cancellation of $\ell = 4$ modes is not taken into account by his fits.

Clearly, there is no agreement about G185−32's seismology. Therefore, we also studied G185−32 in the same way as we did for G117−B15A, to check if our method agrees with any other previous mode identifications. In Table 4, we show G185−32's atmospheric parameters derived from different methods.

Our model computes only $m = 0$ modes, because we include neither rotation nor magnetic field, which would split modes with different values of m. Metcalfe (2003) concluded that the families of solutions are the same even if we use the wrong m mode, for slow rotators (like pulsating white dwarfs). Once again, it is necessary to exclude the linear combinations in the fit, which is definitely not a trivial task for G185−32. In Table 5, we list the periodicities published by Castanheira et al. (2004), their optical amplitudes, and the linear combinations. As the periods at 537.6, 454.6 and 181.9 s were marginally detected, we did not include them in our seismological analysis.

Table 5. All periodicities detected for the star G185−32, with the mode identification of the linear combinations and harmonics of the highest-amplitude periodicity. The question mark is used for the modes marginally detected, which were not used in our seismological studies.

Periodicities (s)	Amplitude (mma)	Identification
651.70	0.67	f_1
560.77	0.09	$f_3 - f_1$
537.59	0.57	(?)
454.56	0.38	(?)
370.21	1.62	f_2
300.60	1.04	f_3
266.17	0.46	f_4
215.74	1.93	f_5
181.90	0.03	(?)
148.45	0.57	$f_7 - f_6$
141.87	1.43	f_6 ($\sim 3f_5/2$)
72.54	0.93	f_7 ($\sim 3\,f_5$)
70.93	0.69	$2 \times f_6$

Table 4. Independent atmospheric determinations for G185−32.

Method	$T_{\rm eff}$ (K)	$\log g$ (in cgs)	M (${\rm M}_\odot$)	Spectroscopic reference
Optical spectra	$12\,130 \pm 200$	8.05 ± 0.05	0.64 ± 0.03	Bergeron et al. (2004)
UV spectra + V mag	$11\,820 \pm 200$	7.92 ± 0.10	0.57 ± 0.05	Koester & Allard (2000)
Many methods	$11\,960 \pm 80$	8.02 ± 0.04	0.62 ± 0.02	Castanheira et al. (2004)

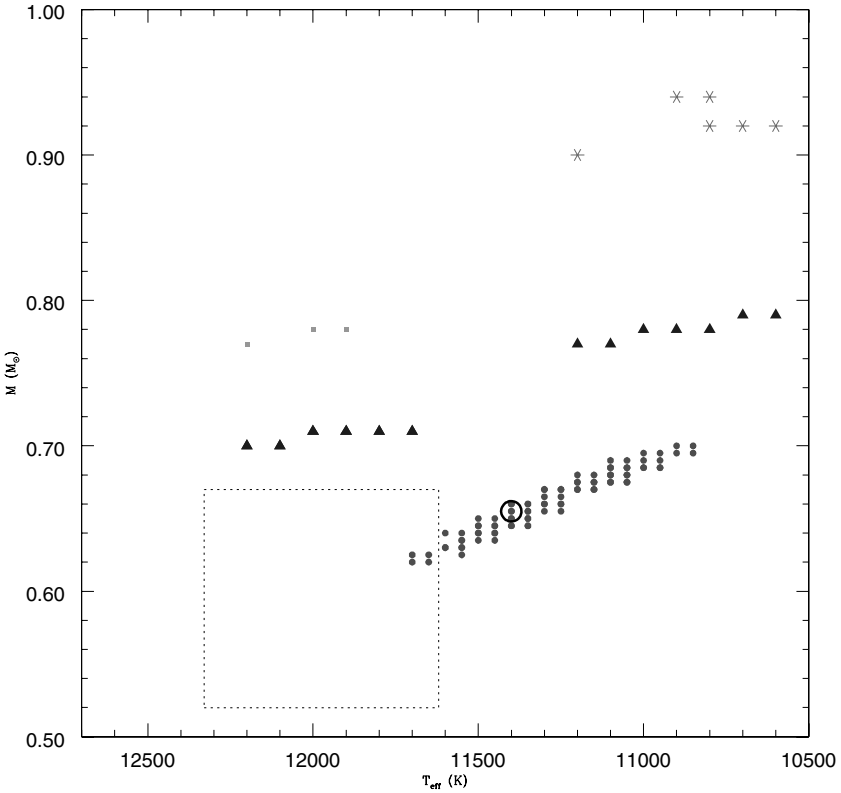

Figure 8. Results of the fit of the pulsation modes for the star G185−32. The (red) circles are the solutions for $M_{\rm He} = 10^{-2}\,M_*$, the (blue) triangles for $M_{\rm He} = 10^{-2.5}\,M_*$, the (green) squares for $M_{\rm He} = 10^{-3}\,M_*$, and the (magenta) asterisks for $M_{\rm He} = 10^{-3.5}\,M_*$. The dotted line box limits the region of the independent temperature and mass determinations listed in Table 4 and the open circle shows the location of the minimum for this family of solutions.

Table 6. Absolute minima of the various families of solutions of the seismological analysis for the star G185−32. Values in bold represent seismological solution that better agrees with external methods. All points are below S cut off.

Symbol in plot 8	$T_{\rm eff}$ (K)	M ($M_\odot$)	$-\log M_{\rm H}$	$-\log M_{\rm He}$	S (s)	Modes (ℓ, k)
1. Circles (red)	**11 400**	**0.655**	**7**	**2**	0.75	216.0(1, 1), 262.3(1, 2) 298.3(1, 3), 369.5(1, 4) 654.5(1, 10)
2. Triangles (blue)	10 900	0.78	2.5	5	0.85	215.1(1, 2), 258.0(1, 3) 303.2(1, 4), 370.4(1, 6) 649.6(1, 13)
3. Squares (green)	11 900	0.78	3	5	1.94	216.7(1, 2), 258.2(1, 3) 303.7(1, 4), 370.2(1, 6) 634.9(1, 12)
4. Asterisks (magenta)	10 700	0.92	3.5	6	0.93	215.7(1, 2), 260.9(1, 3) 301.6(1, 4), 368.7(1, 6) 655.0(1, 14)

The first attempt was to use only the modes longer than 215 s (from f_1 to f_5), which is a very similar analysis to that of G117−B15A. In Fig. 8, we show all the solutions for $S < 2$ s, assuming that all modes are $\ell = 1$. The minima of the families of solutions are listed in Table 6.

The closest seismological solution to the previous atmospheric determinations is solution (1): $T_{\rm eff} = 11\,400$ K, $M = 0.655\,{\rm M}_\odot$, $M_{\rm H} = 10^{-7}\,M_*$ and $M_{\rm H} = 10^{-2}\,M_*$. In this model, a 71.43-s $\ell = 4, k = 1$ mode is present. There is also an $\ell = 4, k = 5$ mode at 150.9 s, a substantial difference of 9 s from the observed periodicity at 141.8 s. The lack of a mode closer to the observed value in the best model supports the proposal that this periodicity is, in fact, a non-linear effect. On the other hand, Bradley's (2006) suggestion for the 72-s mode to be $\ell = 4$ agrees with our seismological study. Despite the fact that its observed amplitude is not consistent with an $\ell = 4$ mode, because of the large geometrical cancellation expected, the amplitude could have been amplified by the resonance with the harmonic of the main mode.

The best fits for G117−B15A and G185−32 indicate that these stars have a very similar structure: $M_{\rm H} = 10^{-7}\,M_*$ and $M_{\rm He} = 10^{-2}\,M_*$. The total masses are a little different though. As G117−B15A has $\langle P\rangle = 233.1$ s and G185−32 has $\langle P\rangle = 280.4$ s, their seismological temperatures are consistent with the second being a little cooler than the first one (as in Mukadam et al. 2006).

Table 7. Independent determinations for the atmospheric parameters of G226−29.

Method	$T_{\rm eff}$ (K)	M ($M_\odot$)	Spectroscopic reference
LPT optical spectra	12 460 ± 200	0.79 ± 0.03	Bergeron et al. (2004)
LPT optical spectra	12 260 ± 200	0.81 ± 0.03	Gianninas, Bergeron & Fontaine (2005)
UV spectra + V mag	12 050 ± 160	0.73 ± 0.07	Koester & Allard (2000)

3.3 G226−29: poor man's seismology

G226−29 is the brightest known ZZ Ceti ($V = 12.22$) and the closest one too ($d \sim 12$ pc). This star is one of the (if not the) hottest ZZ Ceti stars, according to temperature and mass determinations listed in Table 7.

On the other hand, G226−29 is the poorest star in terms of observed modes. Kepler et al. (1995) reported the detection, even on a Whole Earth Telescope (WET) campaign, of a single triplet, with periods very close to 109 s. The central component is at 109.278 s, the mode we used to study the internal structure of this star. The presence of a triplet is consistent with rotational splitting of an $\ell = 1$ mode. The $\ell = 1$ identification is also reinforced by the UV chromatic amplitude variation (see Kepler et al. 2000, for further discussions).

The total uncertainty used in our fit is S=1 s, because the models are not more accurate than this, due to the uncertainties in the physical parameters, even though the observations for this star are more precise. In Fig. 9, we show the families of solutions for different He layer masses, identified by different symbols.

Even with only one excited mode, there are no solutions for masses lower than 0.7 $M_\odot$! This result shows that seismology is indeed a powerful tool to study stellar interiors and that some information can be obtained even from a single mode.

Using the previous atmospheric determinations, the mass range is between 0.66 and 0.84 $M_\odot$ and temperature, between 11 890 and 12 660 K. In Table 8, we list the minima of the only two families of solution within this interval. The two possible seismological solutions differ by 0.005 $M_\odot$ in mass and 300 K in temperature. The H layer can only be thick and around $10^{-4.5}\,M_*$, and the He layer mass can only be between 10^{-2} and $10^{-2.5}\,M_*$ (modulo the core profile).

3.4 HL Tau76: rich man's seismology

HL Tau76 is an example of a red edge pulsator, showing many periodicities. Because of the large number of modes, linear combinations and harmonics are likely to appear. This can complicate the identification of the fundamental modes. However, when daughter modes are detected, the parent modes have to be excited as well, and

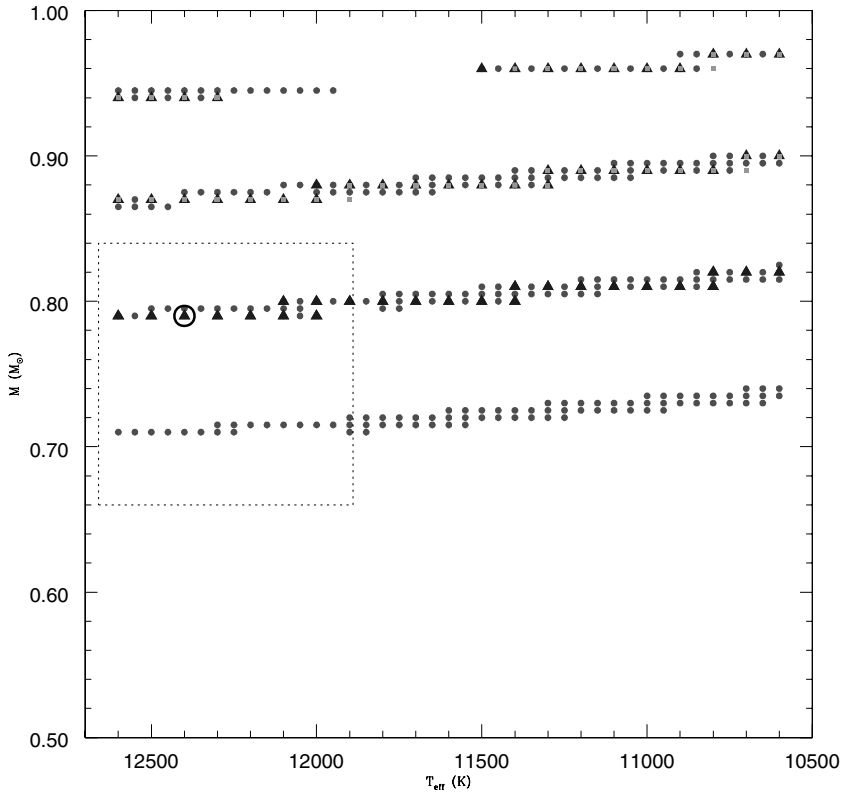

Figure 9. Fit results for the pulsation mode of the star G226−29. The (red) circles are the solutions for $M_{\rm He} = 10^{-2}\,M_*$, the (blue) triangles for $M_{\rm He} = 10^{-2.5}\,M_*$, and the (green) squares for $M_{\rm He} = 10^{-3}\,M_*$. There is no solution for $M_{\rm He} = 10^{-3.5}\,M_*$. The conclusion is that the stellar mass should be high and that the He layer should be thick. The dotted line box limits the region of the independent temperature and mass determinations listed in Table 8 and the open circle shows the location of the minimum for this family of solutions.

Table 8. Absolute minima of the possible families of solutions from the seismological analysis of G226−29.

Symbol in plot 9	$T_{\rm eff}$ (K)	M ($M_\odot$)	$-\log M_{\rm H}$	$-\log M_{\rm He}$	S (s)	Modes (ℓ, k)
1. Circles (red)	12 100	0.795	4.5	2	0.047	109.33(1, 1)
2. Triangles (blue)	**12 400**	**0.79**	**4.5**	**2.5**	0.001	109, 28(1.1)

Table 9. Independent determinations for the atmospheric parameters for the star HL Tau76.

Method	$T_{\rm eff}$ (K)	$\log g$ (in cgs)	M ($M_\odot$)	Spectroscopic reference
LPT optical spectra	11 450 ± 200	7.89 ± 0.05	0.55 ± 0.02	Bergeron et al. (2004)
UBV colours	10 500 ± 500	7.5 ± 0.5	0.36 ± 0.19	This paper

Table 10. All detected modes for the star HL Tau76, in different years of observations (Dolez et al. 2006).

Periodicities (s)	Amplitude (mma)	Identification
382.47 ± 0.02	16.47	f_1
449.8 ± 0.13	6.7	f_2
492.12 ± 0.11	7.12	f_3
540.95 ± 0.01	28.45	f_4
596.79 ± 0.03	14.40	f_5
664.21 ± 0.03	14.94	f_6
781.0 ± 0.07	9.1	f_7
799.10 ± 0.21	5.19	f_8
933.64 ± 1	2.40	f_9
976.38 ± 0.14	6.46	f_{10}
1064.97 ± 0.05	11.30	f_{11}
1390.84 ± 0.37	3.92	f_{12}

the amplitude behaviour of the daughter modes has to be similar to that of the parent modes. On the other hand, the dramatic observed seasonal changes in the pulsation spectra also make the search for parent modes more difficult. Fortunately, the excited modes reappear at the same frequencies as in the previous seasons. Considering that the transition zones between the layers are not sharp and that both convection zone depth and temperature change during the pulsation cycle (e.g. Montgomery 2005), a mode can appear at 600 and 615 s, depending on when the star is observed.

Another characteristic of red edge pulsators is the normally high amplitude of the observed modes. The ionization zone is getting deeper as the star cools down; the energy transported by pulsations is larger. For these stars, $T_{\rm eff}$ can vary up to 500 K (Robinson, Kepler & Nather 1982), almost half of the size of the ZZ Ceti instability strip (∼1200 K). Because of that, it is necessary to average out the stellar pulsation period when deriving an $T_{\rm eff}$ from spectral fluxes.

Table 9 shows the spectroscopic determinations for HL Tau76 and our estimate from the colours. We used the optical spectra determination as the main guide, allowing our searches to be within three times the published uncertainties. This range includes also the colour determinations.

The list of HL Tau76 independent modes and their uncertainties calculated from the amplitudes is shown in Table 10. The modes were published by Dolez et al. (2006), and were detected in two WET campaigns.

We compared the observed modes with our model grid, assuming first that all modes are $\ell = 1$. The families of solutions are shown in Fig. 10; in this case, the cut-off is $S < 5$ s. The minima of each family of solutions that is in agreement with the external atmospheric determination are listed in Table 11.

The seismological study of the star HL Tau76 shows the difficulties of determining the internal characteristics of the star when its atmospheric parameters are not well established and when the star is close to the red edge, even though a large number of modes is excited. However, there is another piece of information which has not been used for the hotter stars, but that is very suitable for red edge pulsators: period spacing (ΔP). For $k > 5$ modes, ΔP value will approach the asymptotic limit. This is not the case for blue edge pulsators, where only low-k modes are observed. From the expression

$$\Delta P \propto \frac{1}{[\ell(\ell+1)]^{1/2}}, \tag{3}$$

ΔP is larger for $\ell = 1$ modes than for $\ell = 2$ ($\Delta P_{\ell=1}/\Delta P_{\ell=2} = 1.73$). In Table 12, we list the differences in seconds between the modes.

We found only two repeating values: ∼45 and ∼65 s, which should be representative of ℓ=2 and 1 modes, respectively. Also, the ΔP between high-amplitude modes is longer than that for low-amplitude modes, consistent with the geometrical cancellation effects. The high-amplitude modes should be $\ell = 1$, while the small-amplitude ones, $\ell = 2$. Therefore, we fixed the modes at 382.47, 449.8, 540.95, 596.79, 664.21, 781.0 and 1064.97 s as $\ell = 1$, and the other ones were allowed to fit either $\ell = 2$ or 1. The families of solutions are plotted in Fig. 11 and the minima for each solution are given in Table 13.

Solutions (1) and (3) are for masses different from the spectroscopic value. All the other solutions have a thin H layer. Solution (5) is the closest to previous determinations, with $T_{\rm eff} = 11\,100$ K, $M = 0.56\,M_\odot$, $M_{\rm H} = 10^{-8}\,M_*$ and $M_{\rm He} = 10^{-3.5}\,M_*$.

3.5 BPM37093: for millionaires

BPM37093, a high-mass white dwarf with $1.1 \pm 0.05\,M_\odot$ (e.g. Bergeron et al. 2004), was discovered to be a ZZ Ceti by Kanaan et al. (1992). Massive white dwarfs have even higher densities and pressures than normal white dwarfs. According to the evolutionary models, white dwarfs with $M > 1\,M_\odot$ have a significant crystallized portion already when they reach the ZZ Ceti instability strip (Wood 1992; Winget et al. 1997; Córsico et al. 2005).

Like the stars at the red edge, BPM37093 shows irregularities in its pulsational spectra. The nine independent modes detected by

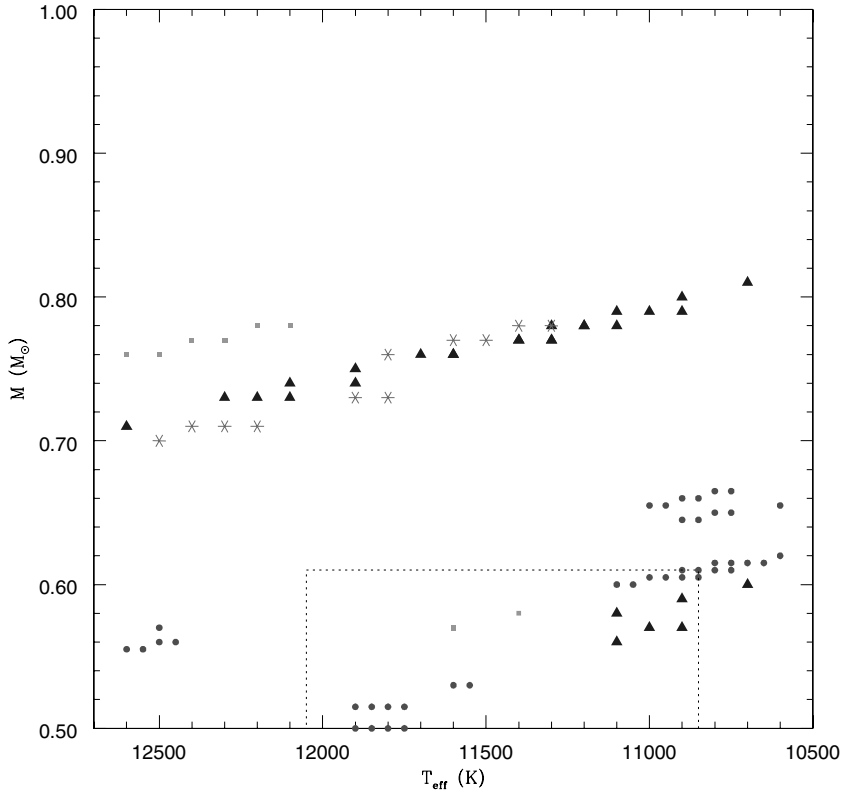

Figure 10. Results from the fit of the pulsation modes of the star HL Tau76 to the models. The (red) circles are the solutions for $M_{\rm He} = 10^{-2}\ M_*$, the (blue) triangles for $M_{\rm He} = 10^{-2.5}\ M_*$, the (green) squares for $M_{\rm He} = 10^{-3}\ M_*$, and the (magenta) asterisks for $M_{\rm He} = 10^{-3.5}\ M_*$. The dotted line box limits the region of the independent temperature and mass determinations listed in Table 9.

Table 11. Absolute minima for the various families of solutions from the seismological analysis for the star HL Tau76, for the values closest to the spectroscopic solutions.

Symbol in plot 9	$T_{\rm eff}$ (K)	M ($M_\odot$)	$-\log M_{\rm H}$	$-\log M_{\rm He}$	S (s)
1. Circles (red)	11 900	0.515	6	2	4.63
2. Circles (red)	10 600	0.62	4	2	4.07
3. Triangles (blue)	10 900	0.59	6.5	2.5	4.45
4. Squares (green)	11 400	0.58	6.5	3	4.76

Table 12. Difference between consecutive modes for the star HL Tau76. $\Delta P \sim 45$ s is probably representative of differences between $\ell = 2$ modes, while $\Delta P \sim 65$ s for $\ell = 1$.

ΔP (s)	Modes
67	$f_2 - f_1$
43	$f_3 - f_2$
49	$f_4 - f_3$
56	$f_5 - f_4$
67	$f_6 - f_5$
2×68	$f_7 - f_6$
18	$f_8 - f_7$
3×46	$f_9 - f_8$
43	$f_{10} - f_9$
2×44	$f_{11} - f_{10}$
325	$f_{12} - f_{11}$

Kanaan et al. (2005), used in our seismological studies, are listed in Table 14.

Metcalfe, Montgomery & Kanaan (2004) labelled most of the modes as $\ell = 2$, due to the small period spacing, $\langle \Delta P \rangle = 17.6 \pm 1.1$ s. They used fixed masses of 1.0, 1.03 and 1.1 $M_\odot$, to search for the best temperatures inside the instability strip, with a model-fitting method using a genetic algorithm. They explored only two possibilities of H and He layer masses: the range between 10^{-4} and 10^{-8} M_* for H and 10^{-2} and 10^{-4} M_* for He, and the self-consistent results from massive stars evolutionary models, $10^{-5.8}$ and $10^{-3.1}$ M_* (Althaus et al. 2003). They varied the crystallized portion of a pure O nucleus. Their best fit indicates that 90 per cent of the stellar mass should be already crystallized.

There are only a few known high-mass white dwarfs (Kepler et al. 2007), mostly because they are rare, evolve fast, and have low luminosity. Therefore, the study of BPM37093 is very important to constrain the evolution of massive progenitors. Up to date, it is the only $M > 1\ M_\odot$ ZZ Ceti with reliable mass determinations.

Our initial model grid did not include masses higher than 1 $M_\odot$, which is the case for BPM37093. As a first test, we searched for solutions inside the existing grid, but no solution was found even assuming that all modes are $\ell = 2$. We expanded our model grid, including masses from 1.0 to 1.1 $M_\odot$, in 0.01-$M_\odot$ steps. Because we were calculating high-mass models, we used a pure O core, as expected from self-consistent evolutionary calculations (Iben 1990; Iben, Ritossa & Garcia-Berro 1997).

Using the high-mass grid, there is no solution if all modes were required to be $\ell = 1$. The period spacing and the low detected amplitudes are consistent with $\ell = 2$ modes. The minima of the families of the seismological solutions are given in Table 15.

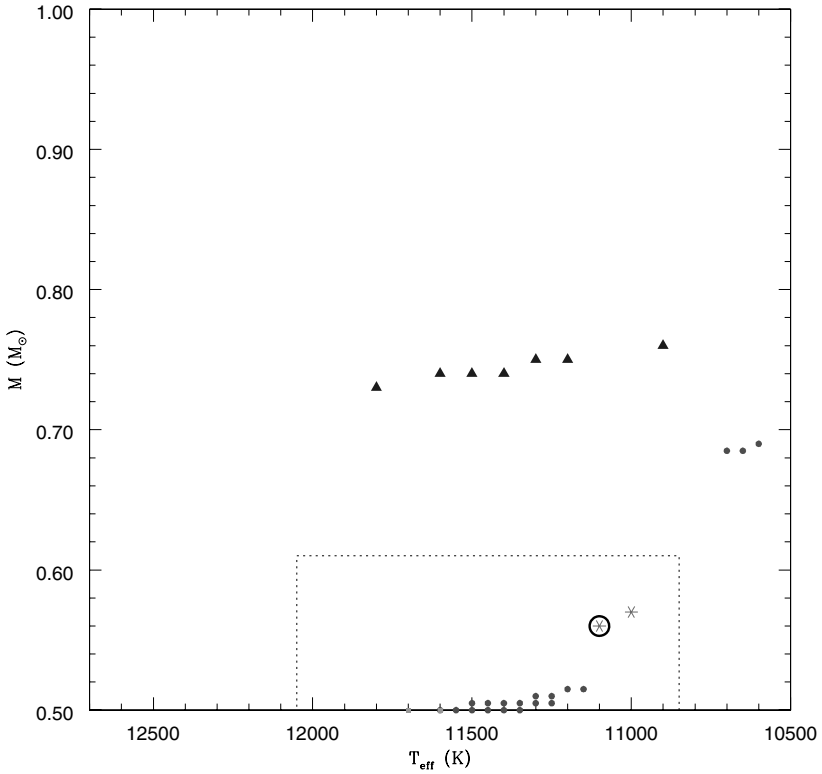

Figure 11. Results of the fit of the pulsation modes for the star HL Tau76 to the models. The (red) circles are the solutions for $M_{\rm He} = 10^{-2}\ M_*$, the (blue) triangles for $M_{\rm He} = 10^{-2.5}\ M_*$, the (green) squares for $M_{\rm He} = 10^{-3}\ M_*$, and the (magenta) asterisks for $M_{\rm He} = 10^{-3.5}\ M_*$. The higher amplitude modes and with period spacing of ∼65 s were fixed to $\ell = 1$ and the others could be fitted to $\ell = 2$ modes. The dotted line box limits the region of the independent temperature and mass determinations listed in Table 9 and the open circle shows the location of the minimum for this family of solutions.

Table 13. Absolute minima of the various families of solutions from the seismological studies of HL Tau76, for the values close to the spectroscopic solution. There are other families of solutions if the total mass is above 0.70 $M_\odot$. The dotted line box represents the spectroscopic determination in 3σ.

Symbol in plot 9	$T_{\rm eff}$ (K)	M ($M_\odot$)	$-\log M_{\rm H}$	$-\log M_{\rm He}$	S (s)	Modes (ℓ, k)
1. Circles (red)	10 600	0.69	8	2	3.75	
2. Circles (red)	11 500	0.50	7.5	2	2.37	
3. Triangles (blue)	11 500	0.74	5	2.5	3.39	
4. Squares (green)	11 700	0.50	7.5	3	3.70	
5. Asterisks (magenta)	**11 100**	**0.56**	**8**	**3.5**	3.20	395.9(1,3), 461.7(1,5) 490, 2(2, 11), 539.8(1, 6) 596.4(1, 7), 667.2(1, 8) 767.0(1, 10), 789.0(2, 20) 924.3(2, 24), 993.4(2, 26) 1054.9(1, 15), 1397.5(1, 21)

Table 14. Modes for BPM37093.

Periodicities (s)	Amplitudes (mma)
511.7	0.68
531.1	1.16
548.8	0.98
564.0	1.03
582.0	1.03
600.7	0.88
613.5	1.13
635.1	1.53
660.8	0.48

Notes. Detected modes in the star BPM37093, as listed in Kanaan et al. (2005).

According to our seismological studies, the 613.5-s mode, the third largest one, always fits better by $\ell = 1$, the 582.0-s mode can be either $\ell = 1$ or 2, and all the other modes are better fitted by $\ell = 2$. Our results are in agreement with the analysis of Metcalfe et al. (2004).

Even though it is not possible to determine the He layer mass, we can constrain the total stellar masses as high ($M > 1\,M_\odot$), temperatures between 11 600 and 11 800 K (only 200 K of external uncertainty), and H layer mass between 10^{-6} and $10^{-7}\ M_*$, consistent with seismological determinations from Althaus et al. (2003). Our seismological determinations for the high-mass red edge, $T_{\rm eff}$, are also in theoretical and observational agreement with this to be hotter than the low-mass red edge.

Table 15. Absolute minima for the various families of solutions of the seismological analysis for the star BPM37093.

$T_{\rm eff}$ (K)	M ($M_\odot$)	$-\log M_{\rm H}$	$-\log M_{\rm He}$	S (s)	Modes (ℓ, k)
11 800	1.10	7	2	0.99	515.1(2, 27), 531.7(2, 28), 548.5(2, 29), 566.5(2, 30) 582.6(1, 17), 601.9(2, 32), 613.1(1, 18), 635.8(2, 34) 653.9(2, 35)
11 700	1.08	6.5	2.5	1.02	514.8(2, 27), 531.8(2, 28), 549.0(2, 29), 566.2(2, 30) 584.0(2, 31), 601.5(2, 32), 614.2(1, 18), 636.2(2, 34) 653.6(2, 35)
11 600	1.07	6	3	1.03	514.8(2, 27), 532.5(2, 28), 549.5(2, 29), 566.8(2, 30) 583.2(1, 17), 601.6(2, 32), 612.9(1, 18), 636.6(2, 34) 654.0(2, 35)
11 800	1.10	6.5	3.5	1.15	514.5(2, 27), 532.0(2, 28), 549.7(2, 29), 566.8(2, 30) 584.3(2, 31), 601.5(2, 32), 614.6(1, 18), 636.6(2, 34) 654, 2(2, 35)

4 FINAL DISCUSSIONS AND CONCLUSIONS

In this work, we have built and explored an extensive model grid, which calculates all possible modes that can be excited for a given internal structure at certain temperatures. We have also developed an independent technique of model fitting to compare the observed periods to the calculated periods. In our approach, we used the external temperature and mass determinations to guide the seismological solutions, but we never limited the search to the uncertainty range of the spectroscopic determinations. G117−B15A was the best star to test our seismological approach.

Our seismological study of a few ZZ Ceti stars is a clear evidence that seismology is really a powerful tool in the study of stellar evolution. Even for the stars with few excited modes, it is possible to determine some characteristics of their interior. For G226−29, with only one detected mode it was possible to restrict the mass to be above 0.7 $M_\odot$. Combined with reliable values for temperature and mass, three internal parameters could be determined, because the modes do not show an asymptotic behaviour, that is, they are more sensitive to the structure of the star.

The study of G185−32 was the motivation to include the relative amplitudes to give weights to the observed periods in the fits. The idea is that the high-amplitude modes should be present in the best models. Our conclusion is that the observed amplitudes should be taken into account, even when one calculates the modes from an adiabatic model.

As a red edge example, we analysed HL Tau76. In this case, the period spacing was a very useful tool, especially because of the asymptotic behaviour of the modes when they are larger. This analysis was consistent with the relative amplitudes between the $\ell = 1$ and 2 modes.

The success of the application of our approach to these five stars, including also the well-studied BPM37093, encourages us to do seismology of all other known ZZ Ceti stars. This is the topic of the second paper of this series, where the results for the whole class will be presented and discussed.

ACKNOWLEDGMENTS

We acknowledge support from the CNPq-Brazil. We also acknowledge Travis S. Metcalfe for making available his scripts to calculate the model grid used in this work and Agnes Bischoff-Kim for sharing her version of the model with the Salaris profile.

REFERENCES

Althaus L. G., Serenelli A. M., Córsico A. H., Montgomery M. H., 2003, A&A, 404, 593
Benvenuto O. G., Córsico A. H., Althaus L. G., Serenelli A. M., 2002, MNRAS, 332, 399
Bergeron P., Fontaine G., Billères M., Boudreault S., Green E. M., 2004, ApJ, 600, 404
Bohm K. H., Cassinelli J., 1971, A&A, 12, 21
Bradley P. A., 1998, ApJS, 116, 307
Bradley P. A., 2006, Memorie della Societa Astronomica Italiana, 77, 437
Bradley P. A., Winget D. E., 1994, ApJ, 430, 850
Brassard P., Fontaine G., Wesemael F., Kawaler S. D., Tassoul M., 1991, ApJ, 367, 601
Castanheira B. G. et al., 2004, A&A, 413, 623
Clemens J. C., van Kerkwijk M. H., Wu Y., 2000, MNRAS, 314, 220
Córsico A. H., Benvenuto O. G., Althaus L. G., Isern J., García-Berro E., 2001, New Astron., 6, 197
Córsico A. H., Althaus L. G., Montgomery M. H., García-Berro E., 2005, in Koester D., Moehler S., eds, ASP Conf. Ser. Vol. 334, 14th European Workshop on White Dwarfs. Astron. Soc. Pac., San Francisco, p. 537
Dolez N. et al., 2006, A&A, 446, 237
Fontaine G., Graboske H. C., Jr, van Horn H. M., 1977, ApJS, 35, 293
Fontaine G., Bergeron P., Brassard P., Wesemael F., Vauclair G., Kawaler S. D., Grauer A. D., Winget D. E., 1991, ApJ, 378, L49
Gianninas A., Bergeron P., Fontaine G., 2005, ApJ, 631, 1100
Hansen B. M. S. et al., 2002, ApJ, 574, L155
Hansen B. M. S. et al., 2007, ApJ, 671, 380
Hine B. P. A. I., 1988, PhD thesis, Univ. Texas, Austin
Iben I. J., 1990, in Cacciari C., Clementini G., eds, ASP Conf. Ser. Vol. 11, Confrontation Between Stellar Pulsation and Evolution. Astron. Soc. Pac., San Francisco, p. 483
Iben I. J., Ritossa C., Garcia-Berro E., 1997, ApJ, 489, 772
Iglesias C. A., Rogers F. J., 1996, ApJ, 464, 943
Itoh N., Hayashi H., Nishikawa A., Kohyama Y., 1996, ApJS, 102, 411
Kalirai J. S., Bergeron P., Hansen B. M. S., Kelson D. D., Reitzel D. B., Rich R. M., Richer H. B., 2007, ApJ, 671, 798
Kanaan A., Kepler S. O., Giovannini O., Diaz M., 1992, ApJ, 390, L89
Kanaan A. et al., 2005, A&A, 432, 219
Kawaler S. D., Winget D. E., Iben I., Jr, Hansen C. J., 1986, ApJ, 302, 530
Kepler S. O., Nather R. E., McGraw J. T., Robinson E. L., 1982, ApJ, 254, 676
Kepler S. O. et al., 1995, ApJ, 447, 874
Kepler S. O., Robinson E. L., Koester D., Clemens J. C., Nather R. E., Jiang X. J., 2000, ApJ, 539, 379
Kepler S. O. et al., 2003, A&A, 401, 639
Kepler S. O. et al., 2005, ApJ, 634, 1311
Kepler S. O., Kleinman S. J., Nitta A., Koester D., Castanheira B. G., Giovannini O., Costa A. F. M., Althaus L., 2007, MNRAS, 375, 1315

Kim A., Montgomery M. H., Winget D. E., 2006, in Kannapan S. J., Redfield S., Kessler-Silacci J. E., Landriau M., Drory N., eds, ASP Conf. Ser. Vol. 352, New Horizons in Astronomy: Frank N. Bash Symposium. Astron. Soc. Pac., San Francisco, p. 253
Koester D., Allard N. F., 2000, Baltic Astron., 9, 119
Kotak R., van Kerkwijk M. H., Clemens J. C., 2004, A&A, 413, 301
Lamb D. Q., 1974, ApJ, 192, L129
Lamb D. Q., van Horn H. M., 1975, ApJ, 200, 306
McGraw J. T., Robinson E. L., 1976, ApJ, 205, L155
McGraw J. T., Fontaine G., Lacombe P., Dearborn D. S. P., Gustafson J., Starrfield S. G., 1981, ApJ, 250, 349
Metcalfe T. S., 2003, Baltic Astron., 12, 247
Metcalfe T. S., 2005, MNRAS, 363, L86
Metcalfe T. S., Montgomery M. H., Kanaan A., 2004, ApJ, 605, L133
Montgomery M. H., 1998, PhD thesis, Univ. Texas, Austin
Montgomery M. H., 2005, ApJ, 633, 1142
Mukadam A. S., Montgomery M. H., Winget D. E., Kepler S. O., Clemens J. C., 2006, ApJ, 640, 956
Nather R. E., Mukadam A. S., 2004, ApJ, 605, 846
Pech D., Vauclair G., 2006, A&A, 453, 219
Robinson E. L., Kepler S. O., Nather R. E., 1982, ApJ, 259, 219
Robinson E. L. et al., 1995, ApJ, 438, 908
Salaris M., Dominguez I., Garcia-Berro E., Hernanz M., Isern J., Mochkovitch R., 1997, ApJ, 486, 413
Thompson S. E., Clemens J. C., van Kerkwijk M. H., O'Brien M. S., Koester D., 2004, ApJ, 610, 1001
Wegner G., Reid I. N., 1991, ApJ, 375, 674
Winget D. E., van Horn H. M., Hansen C. J., 1981, ApJ, 245, L33
Winget D. E., Hansen C. J., Liebert J., van Horn H. M., Fontaine G., Nather R. E., Kepler S. O., Lamb D. Q., 1987, ApJ, 315, L77
Winget D. E. et al., 1994, ApJ, 430, 839
Winget D. E., Kepler S. O., Kanaan A., Montgomery M. H., Giovannini O., 1997, ApJ, 487, L191
Winget D. E., Sullivan D. J., Metcalfe T. S., Kawaler S. D., Montgomery M. H., 2004, ApJ, 602, L109
Wood M. A., 1990, PhD thesis, Univ. Texas, Austin
Wood M. A., 1992, ApJ, 386, 539
Wu Y., 2001, MNRAS, 323, 248
Yeates C. M., Clemens J. C., Thompson S. E., Mullally F., 2005, ApJ, 635, 1239
Zhang E.-H., Robinson E. L., Nather R. E., 1986, ApJ, 305, 740

This paper has been typeset from a TEX/LATEX file prepared by the author.